Influence of the Oxidatively Damaged Adduct 8-Oxodeoxyguanosine on the Conformation, Energetics, and Thermodynamic Stability of a DNA Duplex†

G. Eric Plum,‡ Arthur P. Grollman,§ Francis Johnson,§ and Kenneth J. Breslauer*,‡

Department of Chemistry, Rutgers, The State University of New Jersey, New Brunswick, New Jersey 08903, and Department of Pharmacological Sciences, State University of New York at Stony Brook, Stony Brook, New York 11794

Received August 17, 1995; Revised Manuscript Received October 18, 1995®

ABSTRACT: As part of an overall program to characterize the impact of mutagenic lesions on the physiochemical properties of DNA, we report here the results of a comparative spectroscopic and calorimetric study on a family of DNA duplexes both with and without the oxidative lesion 2′-deoxy-7-hydro-8-oxoguanosine (8-oxodG). Specifically, we have studied a family of eight 13-mer duplexes of the form [5′-GCGTAC[G* or G]CATGCG-3′]·[3′-CGCATG[C, A, T, or G]GTACGC-5′] in which G* is the 8-oxodG lesion. These eight duplexes, which we designate by the identity of the variable central base pair (e.g., G*C), reflect two subsets: four duplexes in which the modified guanine base is positioned opposite each of the four possible canonical residues (G*C, G*A, G*G, G*T) and the corresponding four "control" duplexes in which the guanine is not modified (GC, GA, GG, GT). The data derived from our spectroscopic and calorimetric measurements on these eight duplexes allow us to evaluate the influence of the 8-oxodG lesion, as well as the base opposite the lesion, on the conformation, the thermal and thermodynamic stability, and the melting thermodynamics of the host DNA duplex. We find that modification of dG to 8-oxodG (G*) does not change the global DNA duplex conformation as judged by circular dichroism spectra. Despite this structural similarity, our data reveal that the dG to dG* modification does influence duplex thermal and thermodynamic properties, some of which depend on the base opposite the lesion. Thus, apparent structural identity does not mean that two duplexes necessarily will exhibit equivalent thermal and/or thermodynamic properties. In general, we find that the thermodynamic effects induced by the lesion (e.g., GC vs G*C) or by mismatched base pairs (e.g., GC vs GG) can result in relatively large changes in enthalpy which are partially or wholly compensated entropically to produce relatively modest changes in free energy. Our data also suggest that the biologically observed differential recognition of 8-oxodG duplexes and the preferential nucleotide insertion opposite 8-oxodG residues cannot be rationalized simply in terms of large thermodynamic differences.

Cellular DNA is susceptible to degradation caused by a variety of reactive oxygen species. Highly reactive oxygen species, such as singlet oxygen, H_2O_2, hydroxyl (•OH) and superoxide (O_2^-) radicals, arise in cells from the actions of ionizing radiation (Hutchinson, 1985), chemical mutagens (Floyd, 1990), and endogenous processes (Halliwell & Gutteridge, 1989). Reaction of oxygen free radicals, most probably •OH (Gajewski et al., 1990), at the C-8 position of 2′-deoxyguanosine is responsible for production of a 2′-deoxy-7-hydro-8-oxoguanosine (8-oxodG)[1] lesion in DNA (Kasai & Nishimura, 1984; Cadet & Berger, 1985; Steenken, 1989). The 6,8-diketo form of this lesion, which predominates under biological conditions (Cho et al., 1990), is shown below.

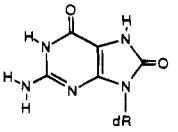

An alternative mechanism by which the 8-oxodG lesion can be introduced into DNA is through corruption of the cellular dGTP pool with 8-oxodGTP, which, in turn, may result in incorporation of 8-oxodG into DNA, with preferential insertion of this lesion occurring opposite dA (Cheng et al., 1992; Maki & Sekaguchi, 1992; Pavlov et al., 1994). The formation and repair of the 8-oxodG adduct has been reviewed extensively (Grollman & Moriya, 1993; Grollman & Shibutani, 1994; Grollman et al., 1994; Demple & Harrison, 1994; Michaels & Miller, 1992; Tchou & Grollman, 1993), so only a brief description is presented below.

Independent of the means by which it forms, the 8-oxodG lesion is mutagenic (Moriya et al., 1991; Shibutani et al., 1991; Wood et al., 1990, 1992; Cheng et al., 1992; Kamiya et al., 1995) and widely distributed in cellular DNA (Kasai & Nishimura, 1991). DNA polymerases can synthesize past an 8-oxodG lesion and incorporate selectively dA and dC residues opposite the lesion (Shibutani et al., 1991; Grollman & Takeshita, 1995). The replicative DNA polymerases (pol α, pol δ, and pol III) favor incorporation of dA, while the repair DNA polymerases (pol I, pol β, and pol γ) favor incorporation of dC. Interestingly, the proofreading function

† This research was supported by NIH Grants GM-23509 and GM-34469 to K.J.B. and CA-47795 to A.P.G.

‡ Rutgers, The State University of New Jersey.

§ State University of New York at Stony Brook.

® Abstract published in *Advance ACS Abstracts,* December 1, 1995.

[1] Abbreviations: 8-oxodG, 2′-deoxy-7-hydro-8-oxoguanosine; CD, circular dichroism; UV, ultraviolet; DSC, differential scanning calorimetry.

0006-2960/95/0434-16148$09.00/0

of DNA polymerase I is not effective against the 8-oxodG·dA base pair (Shibutani et al., 1991). The primary consequence of an unrepaired 8-oxodG, introduced by direct oxidation of dG in DNA, is a G ⇒ T transversion in *Escherichia coli* plasmids and phagemids (Moriya et al., 1991; Wood et al., 1990, 1992; Cheng et al., 1992; Moriya & Grollman, 1993) and in mammalian cells (Bessho et al., 1993a; Moriya 1993; Kamiya et al., 1995). The primary consequence of an 8-oxodG lesion introduced by misincorporation of 8-oxodGTP is an A ⇒ C transversion (Cheng et al., 1992). The proposed complicity of the 8-oxodG lesion in carcinogenesis (Floyd, 1990) and in other age-related degenerative diseases (Fraga et al., 1990) has highlighted this lesion as particularly significant biologically.

Recently, an elaborate scheme for repair of 8-oxodG lesions, which involves several enzymes, has been elucidated in *E. coli* (Michaels et al., 1992a,b). Efficient repair of 8-oxodG opposite dC, dT, and dG is carried out by 8-oxodG DNA glycosylase (Fpg protein/FapydG DNA glycosylase/Mut M protein) (Tchou et al., 1991). The abasic site which results from the enzyme-catalyzed extraction of the damaged 8-oxoguanine base is repaired by the normal excision-repair mechanism (Lindahl, 1990).

The 8-oxodG lesion can appear opposite dA as a result of two processes: misincorporation by DNA polymerase of dA opposite 8-oxodG or insertion of 8-oxodGTP directly opposite dA. When positioned across from dA, the lesion is resistant to repair by 8-oxodG DNA glycosylase (Tchou et al., 1991). The 8-oxodG·dA lesion is, however, repaired by a different DNA glycosylase, Mut Y protein, which extracts the normal adenine base when it is opposite 8-oxodG (Michaels et al., 1992a,b; Moriya & Grollman, 1993) or dG (Au et al., 1989). Repair of the resulting abasic site opposite the 8-oxodG lesion occurs by the usual excision-repair process (Lindahl, 1990). Because the repair polymerases favor incorporation of dC opposite the 8-oxodG lesion, the most probable result of repair is an 8-oxodG·dC lesion which is amenable to repair by 8-oxodG DNA glycosylase as described above.

As already noted, incorporation of the 8-oxodG lesion also can occur by misinsertion of a damaged deoxyguanosine triphosphate (Maki & Sekaguchi, 1992; Cheng et al., 1992; Pavlov et al., 1994). To protect against incorporation of 8-oxodG by this mechanism, a third enzyme, Mut T protein, specifically dephosphorylates 8-oxodGTP, thereby eliminating its incorporation into DNA (Maki & Sekaguchi, 1992). Thus, the mechanism of incorporation and repair of the 8-oxodG lesion depends on the identity of the cross-strand partner residue. Enzyme activities corresponding to those of the Mut M and Mut Y proteins of *E. coli* have been observed in mammalian cell extracts (Bessho et al., 1993a–c; Yeh et al., 1991). Recent studies of human cells have revealed an enzyme similar to Mut T protein (Mo et al., 1992) which participates in an enzyme pathway which rids the nucleotide pool of 8-oxodGTP (Hayakawa et al., 1995).

We have synthesized and incorporated the 8-oxodeoxyguanosine lesion into an oligonucleotide (Bodepudi et al., 1991, 1992; Kouchakdjian et al., 1991) which hybridizes with complementary oligonucleotides to form DNA duplexes. The corresponding unmodified deoxyguanosine containing oligonucleotide is hybridized with the same set of complementary oligonucleotides to form DNA duplexes without the lesion. The nucleotide sequences of these oligonucleotides are shown below.

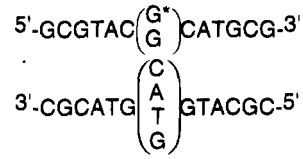

Note that, in this family of duplexes, the 8-oxodG lesion, which we designate G*, is paired opposite each of the four normal deoxynucleotides. The corresponding duplexes containing an unmodified dG residue opposite each of the normal deoxyribonucleotides also were studied for comparison to the lesion containing duplexes. Hereafter, the duplexes are designated by abbreviations which correspond to their central "base pair", i.e., G*C, GC, G*A, GA, etc.

The eight DNA duplexes, four containing the 8-oxodG (G*) lesion and four containing the normal dG residue, were subjected to spectroscopic and calorimetric analysis. Circular dichroism (CD) was employed to characterize the global structure of the duplexes and to evaluate local lesion induced structural perturbations. Temperature-dependent ultraviolet (UV) absorbance and differential scanning calorimetry (DSC) were used to monitor and to characterize the thermally induced duplex to single strand transitions of each duplex. The optical melting experiments provide qualitative insights into the lesion effects on thermal stability, while DSC provides quantitative, model-independent characterizations of effects of the lesion on duplex melting thermodynamics. In the aggregate, the resulting data allow us to define the structural and energetic impacts of the 8-oxodG lesion on duplex properties, while also permitting us to assess whether these lesion-induced alterations can provide insight into biological mechanisms of recognition and repair.

MATERIALS AND METHODS

Preparation of Oligodeoxyribonucleotides and Experimental Conditions

Synthesis of the 8-oxodG phosphoramidite, its incorporation into the oligonucleotide, and subsequent purification of the oligonucleotide were performed as previously described (Bodepudi et al., 1991, 1992; Kouchakdjian et al., 1991). Oligonucleotides without modified guanosine residues were synthesized and purified by standard procedures (Kouchakdjian et al., 1991).

Desalting was accomplished by HPLC on a C_{18} column (Waters Novapak) using an elution gradient of 0.1 M NH_4HCO_3 vs acetonitrile (0 to 20% to 50%). The chromatography was followed by lyophilization. Because the 8-oxodG moiety is susceptible to oxidation in alkali (Bodepudi et al., 1991), the pH of the NH_4HCO_3 solution was reduced to 7.0 by bubbling with CO_2 produced by sublimation of dry ice. Solutions used in HPLC typically were degassed by bubbling with helium. Because degassing would displace dissolved CO_2, thereby raising the pH, degassing of solutions containing the 8-oxodG oligonucleotide was avoided with no apparent impact on the chromatograms.

The residual ammonium ions were exchanged for sodium ions on a gravity flow cation exchange column (Bio-Rad AG 50W-X2), charged with sodium ions. The resulting solution was lyophilized.

All experiments were carried out in 10 mM phosphate buffer containing 1 M NaCl and 0.1 mM EDTA at pH 7.0. The buffer was prepared using appropriate amounts of mono- and disodium phosphate salts, with no adjustment being required to achieve the desired pH.

Extinction Coefficients and Complex Stoichiometry

Molar extinction coefficients (ϵ) for the single-stranded oligonucleotides were determined by phosphate analysis (Snell & Snell, 1949); values at 260 nm and 25 °C are included in Table 1 of the Supporting Information. The stoichiometries of the complexes and their molar extinction coefficients were determined by the method of continuous fractions (Job, 1928; Felsenfeld & Rich, 1957). Complexes were formed by mixing in a 1 cm path length quartz cell, two solutions, each containing a single-stranded oligonucleotide, at a concentration of 5.0×10^{-6} M. The solutions were incubated at 25 °C and the absorbance at 260 nm was measured at 1 min intervals for 20 min. Plots of the absorbance vs the fraction of one of the component strands (data not shown) invariably displayed a break point at a fraction of 0.5, thereby indicating formation of a $m \cdot m$ complex, where m is the number of molecules of each strand. In the absence of any contrary evidence, we assume m is 1. Extinction coefficients of the duplexes so formed were determined from the absorbance at the breakpoint and the known extinction coefficients (concentrations) of the single-stranded oligonucleotides. These ϵ values at 260 nm and 25 °C are included in Table 2 of the Supporting Information.

Circular Dichroism (CD)

CD spectra were collected on an AVIV Model 60 DS spectropolarimeter (AVIV Associates, Lakewood, NJ) at neutral pH and 25 °C in a 0.1 cm path length cell from 200 to 350 nm at 0.5 nm intervals using a 10 s averaging time. The concentrations of DNA duplexes were between 2 and 4 $\times 10^{-5}$ M. To facilitate comparisons, the spectra were normalized in units of molar ellipticity (Cantor & Schimmel, 1980).

Thermal Melting Profiles

Temperature-Dependent Absorbance. Ultraviolet (UV) absorbance monitored thermal melting experiments were performed using a Perkin-Elmer Lambda 4c spectrophotometer interfaced to an Apple Macintosh computer through a National Instruments GPIB-SCSI controller. The temperature was controlled by a Perkin-Elmer digital controller, increased at a rate of 0.5 °C/min, and monitored by a Keithley Model 177 digital multimeter equipped with a Model 1793/6423 IEEE standard output device interfaced to the GPIB-SCSI controller. The temperature and the absorbance values at 260 nm were read and stored at 40 s intervals. The measurements were conducted in 1 cm quartz cuvettes at a DNA duplex concentration of 2.5×10^{-6} M.

The melting temperature, T_m, of the thermally induced order to disorder transition and the van't Hoff enthalpy, ΔH_{vH}^{shape}, of the association reaction were determined as detailed below. Specifically, curves representative of the extent of reaction (α) as a function of temperature were produced from the temperature dependent absorbance profile (Marky & Breslauer, 1987) using baselines extrapolated from least-squares fits of the pre- and posttransition absorbance data. By definition, the temperature at which $\alpha = 0.5$ is T_m. The van't Hoff enthalpy of the transition, ΔH_{vH}^{shape}, was derived from the shape of the transition (Gralla & Crothers, 1973; Marky & Breslauer, 1987). Specifically, derivative curves, $d\alpha/d(1/T)$ vs T, were computed by fitting a third order polynomial (Bevington, 1969) to a sliding window of 11 data points from each α vs $1/T$ curve. Polynomial coefficients so determined where used to estimate the derivative of the curve at the central temperature point of the sliding window. The window was shifted by one point and the fitting process repeated until the entire temperature range was spanned. The temperatures, T_1 and T_2, which corresponded to one half of the maximum of the $d\alpha/d(1/T)$ vs T curve were determined, such that $T_1 < T_{max} < T_2$, and the van't Hoff enthalpy was computed using the relation (Marky & Breslauer, 1987)

$$\Delta H_{vH}^{shape} = -R \ln\left[\frac{\alpha_-(1-\alpha_+)^n}{\alpha_+(1-\alpha_-)^n}\right]\left[\frac{1}{T_1} - \frac{1}{T_2}\right]^{-1} \quad (1)$$

where n is the molecularity of the reaction, R is the gas constant, and

$$\alpha_\pm = \frac{(3+\sqrt{n}) \pm \sqrt{n+6\sqrt{n}+1}}{4(1+\sqrt{n})} \quad (2)$$

Note that when $n = 2$, eq 1 reduces to $\Delta H_{vH}^{shape} = -10.14[(1/T_1) - (1/T_2)]^{-1}$. Estimates of the standard deviation indicated for all data reported here are based on formulae for error propagation, for the appropriate equation. These formulae were derived as described by Bevington (1969).

Another set of van't Hoff enthalpies, ΔH_{vH}^{slope}, were estimated from the dependence of T_{max} on the total oligonucleotide strand concentration, C_t (Marky & Breslauer, 1987; Petersheim & Turner, 1983; Puglisi & Tinoco, 1989). With appropriate modification of the T_m-based equations, van't Hoff thermodynamic data may be extracted from the concentration dependence of T_{max}. For a process of molecularity n, the appropriate equation is

$$\frac{1}{T_{max}} = \frac{(n-1)R}{\Delta H} \ln C_t + \frac{\Delta S - R \ln[(\sqrt{n}+1)^{(n-1)} n^{(n/2-1)}]}{\Delta H} \quad (3)$$

A parallel analysis of T_m and T_{max} data indicates that, within experimental error, the enthalpies extracted from these data are indistinguishable. We use T_{max} because it is somewhat less sensitive to the assignment of baselines. In fact, we found the enthalpy data extracted from T_{max} curves to be independent of whether or not baseline corrections were made prior to differentiation of the melting curves. When ΔH in eq 3 is fixed at ΔH_{cal}, this equation also can be and was used to calculate the effective molecularity of each melting event. Note that the above eqs 1−3 are derived on the basis of an association model; whereas, the data presented in this study are all derived from dissociation reactions. Thus, the reported data differ in sign from those data calculated directly from these equations. The derivation of eq 3 follows that of the complementary equation in terms of T_m (Marky & Breslauer, 1987), with the recognition that, at T_{max}, $\alpha = (\sqrt{n}+1)^{-1}$ (Gralla & Crothers, 1973).

Differential Scanning Calorimetry (DSC). DSC was used to characterize thermodynamically the influence of the lesion on the stability and melting behavior of the DNA duplex (Marky & Breslauer, 1987; Breslauer, 1986; Privalov & Potekhin, 1986; Sturtevant, 1987). As previously emphasized (Marky & Breslauer, 1987; Breslauer, 1986) DSC represents the only experimental method that *directly* yields the *model-independent* thermodynamic (ΔG, ΔH, ΔS, ΔC_p) and extrathermodynamic (size of cooperative melting unit) data of interest.

The transition enthalpies (ΔH) accompanying the disruption of each duplex were obtained by integrating the area under the corresponding DSC curve (C_p^{ex} vs T), because $\Delta H = \int C_p^{ex}\, dT$, where C_p^{ex} denotes the molar "excess" heat capacity relative to solvent. Any heat capacity change associated with each transition was assessed from the difference between the pre- and posttransition baselines. Thus, from each DSC experiment, we obtained directly a measure of the enthalpy change for the thermally induced transition (ΔH) as well as the heat capacity change (ΔC_p). By contrast with indirect van't Hoff analyses of optical data, this calorimetric treatment does not require us to assume that $\Delta C_p = 0$ or to assume that the transition occurs in a two-state manner.

The same calorimetric experiment also provided us with additional information about the influence of the lesion on the nature of the transition. Specifically, the shape of each calorimetric C_p^{ex} vs T curve was evaluated using a two-state model, identical to that used in evaluation of optically observed melting experiments, to calculate the van't Hoff transition enthalpy, ΔH_{vH} (Marky & Breslauer, 1987). Comparison of the model-dependent ΔH_{vH} values (ΔH_{vH}^{cal} or ΔH_{vH}^{shape}) with the model-independent calorimetric enthalpy (ΔH) permitted us to conclude whether intermediate states are significantly populated during the course of each transition and to calculate the impact, if any, of the lesion on the duplex melting cooperativity (Vesnaver et al., 1989; Breslauer, 1986; Privalov & Potekhin, 1986; Sturtevant, 1987). Specifically, if $\Delta H > \Delta H_{vH}$, then the thermally induced transition involves more than two states and the size of the cooperative melting unit can be estimated from the ratio of ΔH_{vH} and ΔH. Only if $\Delta H = \Delta H_{vH}$ can the transition be interpreted in terms of an "all-or-none" model (Marky & Breslauer, 1987; Breslauer, 1986; Privalov & Potekhin, 1986; Sturtevant, 1987). In this way, we were able to evaluate whether the presence of a lesion alters the population of partially bonded states that may arise during thermally induced disruption of each duplex.

All of the calorimetric melting profiles were determined using a Microcal MC-2 differential scanning calorimeter. Lyophilized DNA duplex samples were dissolved in buffer and degassed by vacuum. The concentration of duplex, determined directly, without dilution, by UV absorbance in a 0.035 cm path length cell, was approximately 2×10^{-4} M. Once loaded into the calorimeter cell, the samples were heated from 5 to 100 °C at a rate of 51.6 °C/h. Approximately 15 psi of nitrogen was applied to the sample to inhibit bubble formation and to prevent evaporation. Typically, eight heating cycles where carried out with 1 h between scans. Repeated runs were found to be superimposable; data from 5 to 6 heating cycles were averaged. The instrument was calibrated by measuring the power response to a heat pulse produced by a calibration heater which is integral to the instrument. To correct for the shape of the inherent instrument baseline, five scans with buffer solution in both calorimeter cells were averaged. This averaged instrument baseline was subtracted from the average of 5−6 scans of each DNA sample. Each resulting buffer baseline corrected curve was converted into an apparent molar heat capacity (C_p) vs T curve by dividing by the sample concentration and the sample cell volume. Apparent excess molar heat capacity (C_p^{ex}) vs T curves for each duplex to single strand transition were extracted from the C_p vs T curves by subtraction of the temperature dependence of the heat capacity of the initial duplex and final single strand states. This correction was accomplished by making a linear connection between the pre- and posttransition baselines, a treatment consistent with the near zero heat capacity change for such nucleic acid transitions (Breslauer et al., 1986). The enthalpy of the transition, ΔH_{cal}, was determined by integration of the area between the C_p^{ex} curve and this corrected baseline. The temperature which corresponds to the maximum of C_p^{ex} is T_{max}.

Calculation of the Free Energy of Association. In principle it is possible to calculate the transition free energy directly from DSC data (Marky & Breslauer, 1987). However, in this work we instead combine our optical T_{max} data with our calorimetrically determined ΔH values to calculate apparent association free energies, ΔG, using eq 4, the

$$\Delta G = \Delta H\left(1 - \frac{T}{T_{max}}\right) - RT \ln\left[\left(\frac{\sqrt{n}+1}{C_t}\right)^{(n-1)} n^{(n/2-1)}\right] \quad (4)$$

derivation of which is given in the Supporting Information.

We judge this approach for calculating ΔG to be preferable because it accounts properly for the molecularity of the transition and avoids the coupling and compounding of errors that may result from use of the same data for calculating ΔH and ΔS, a feature which is inherent in the pure DSC approach. Note that, as in eqs 1−3, eq 4 is derived for the association reaction; therefore, data reported in the text differ in sign from those coming directly from this equation. Equation 4 is evaluated using matched pairs of experimentally determined T_{max} and C_t values. When used with the effective molecularity, this relation allows for calculation of an apparent free energy difference at any temperature. Significantly, the ΔG values computed in this fashion are found to be independent of oligonucleotide concentration. These apparent free energy changes are not standard state values. However, the data from which they are calculated were collected under identical conditions, and the activity coefficients of the various oligonucleotides should be virtually identical. Consequently, the differences embodied in $\Delta\Delta G$ values we calculate in this manner should be reliable reflections of the true lesion-induced differences in ΔG.

It should be emphasized that implicit in the comparison of the thermodynamic parameters (ΔH, ΔG) derived from optical or calorimetric data is the reasonable assumption that, at the high temperatures at which the final states are formed, the single strands can be considered to be thermodynamically equivalent. The veracity of this assumption is bolstered by the coalescence of the high temperature CD spectra (data not shown). It also should be noted that, due to potential correlations in the errors of ΔH and ΔG, small differences

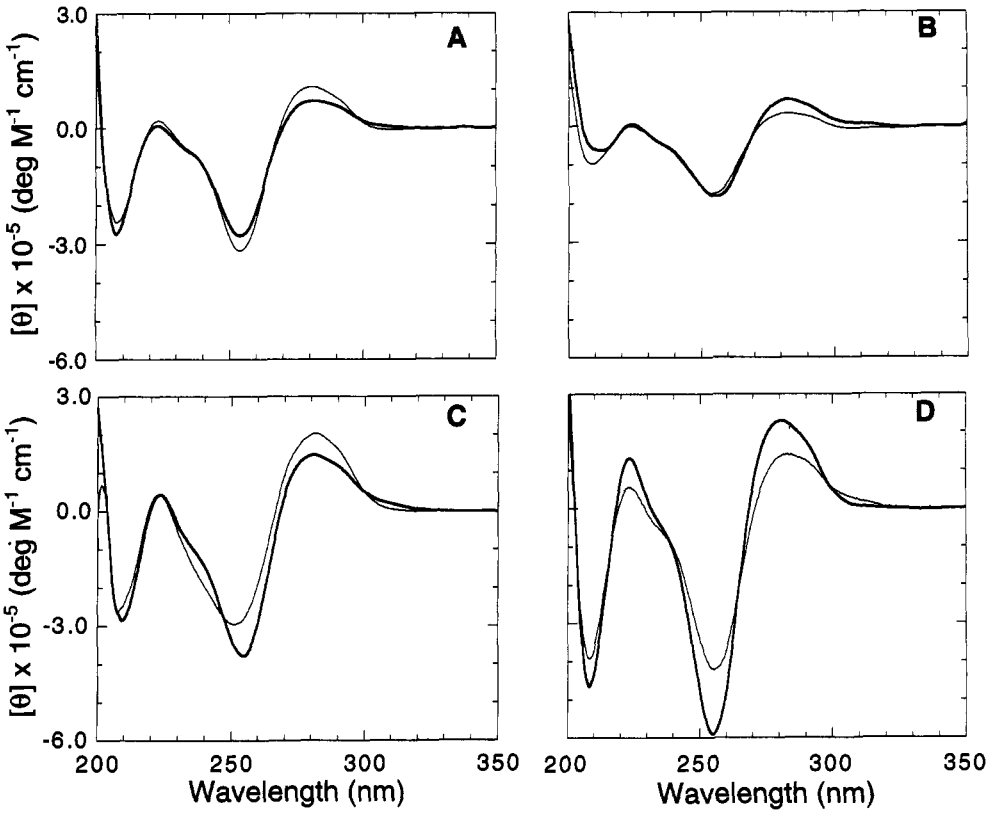

FIGURE 1: Circular dichroism spectra of DNA duplexes with and without the G* lesion: Spectra are in units of molar ellipticity. Lesion containing duplexes are indicated by heavy curves. (A) GC and G*C; (B) GA and G*A; (C) GG and G*G; (D) GT and G*T.

in ΔG may not be statistically significant. Furthermore, uncertainties in ΔC_p amplify errors in ΔG values extrapolated to 25 °C. However, ΔC_p uncertainties are expected to be systematic in origin, thereby not significantly affecting $\Delta\Delta G$ values.

RESULTS AND DISCUSSION

Lesion Effects on Duplex Structure

We have used circular dichroism (CD) spectropolarimetry to evaluate the impact of the lesion and its opposing base on the conformation of the host duplex. In the subsections which follow, we describe the results of these CD studies.

The 8-oxodG Lesion Does Not Alter the Global Duplex Conformation. Inspection of the CD spectra in Figure 1A–D, reveals that, despite quantitative differences, the four duplexes with the dG* lesion (G*C, G*A, G*G, and G*T) and the corresponding four duplexes without the lesion (GC, GA, GG, and GT) all exhibit spectral shapes characteristic of B-like global structures (Bush, 1974), independent of the base opposite the central modified or unmodified G residue. Thus, the presence of the lesion does not alter the global conformation of the host duplexes.

The 8-oxodG Lesion Weakly Perturbs the CD Profile of the Host Duplex. Despite exhibiting CD spectral shapes characteristic of global B-like conformations, comparisons between pairs of duplexes with and without the lesion reveal some quantitative differences. Specifically, only small CD changes occur when dG* replaces dG opposite dC or dA residues (panels A and B), while relatively larger CD alterations occur when dG* replaces dG opposite dG or dT residues (panels C and D). These and other quantitative differences may be indicative of interactions which stabilize alternative base tautomers or may reflect local structural perturbations in the vicinity of the lesion site of the duplex. Alternatively, such quantitative CD changes may be due to more subtle structural perturbations which nevertheless exhibit significant optical effects. Circular dichroism spectropolarimetry, while sensitive to these differences, must defer to NMR and/or X-ray crystallographic techniques for defining the nature of the alterations in molecular structure that may give rise to such quantitative CD detected differences. Consequently, we primarily focus the discussion below on the CD spectra of those duplexes which contain lesions and/or mismatches which have been characterized structurally.

*The GC vs G*C Duplexes: Convergence of Spectral and Structural Data.* In panel A of Figure 1, we see only minimal perturbation in the CD spectrum of the parent GC duplex when dG is replaced by 8-oxodG; in other words, when the GC duplex is converted to the G*C duplex. This observation is consistent with X-ray crystallography (Lipscomb et al., 1995) and NMR evidence (Oda et al., 1991; D. J. Patel, personal communication) which reveal that Watson–Crick B-form geometry is maintained at and adjacent to this lesion site as well as throughout the duplex. This observed compatibility of the lesion with a B-like conformation is not unreasonable. While a variety of tautomers of 8-oxodG are possible (Culp et al., 1989; Cho et al., 1990), under the physiological pH conditions employed in this study (pH 7.0), the lesion exists in the 6,8-diketo form (Culp et al., 1989), a state which is capable of participating in Watson–Crick hydrogen bonding in a manner that does not require either local or global conformational reorganization.

Table 1: Melting Temperatures and van't Hoff Transition Enthalpies Derived from Optical Melting Curves for a Family of DNA Duplexes with and without the 8-oxodG Lesion

duplex	T_m[a] (°C)	ΔH_{vH}^{shape} (kcal/mol)	ΔH_{vH}^{slope} (kcal/mol)
G·C	63.5 ± 0.2	78.9 ± 3.9	98.6 ± 2.2
G*·C	60.3 ± 0.2	81.0 ● 4.7	97.7 ± 2.9
G·A	51.5 ± 0.2	71.5 ± 2.3	88.5 ± 1.5
G*·A	59.1 ± 0.2	83.4 ± 2.3	106.6 ± 2.5
G·G	54.9 ± 0.2	78.2 ± 3.0	79.7 ± 5.5
G*·G	53.2 ± 0.2	79.5 ± 3.3	85.5 ± 4.2
G·T	55.3 ± 0.2	81.3 ± 3.6	86.6 ± 4.2
G*·T	54.3 ± 0.2	82.8 ± 3.4	95.4 ± 7.4

[a] DNA concentration is 5.0×10^{-6} M single strands.

*The GA vs G*A Duplexes: Divergence of Spectral and Structural Data.* Inspection of panel B of Figure 1 reveals only small differences between the CD spectra of the GA and the G*A duplexes. By analogy with the results for the GC and G*C duplexes, it is tempting to conclude from this spectral similarity that no significant alteration in duplex structure occurs when a guanine base opposite an A residue is oxidized to form a dG* lesion site. However, NMR (Kouchakdjian et al., 1991) and X-ray (McAuley-Hecht et al., 1994) studies, although in different sequence contexts, reveal that modification of a guanine base opposite a dA residue to form 8-oxoguanine results in the damaged guanine undergoing a glycosidic rotation from a dG(anti)·dA(anti) conformation (Gao & Patel, 1988) to an 8-oxodG(syn)·dA-(anti) conformation. Apparently, the rather small differences in CD spectra shown in panel B do not reflect strongly this significant local conformational accommodation of the lesion. In short, small differences in CD spectra do not necessarily imply small local structural differences, a conclusion we previously reached in our study of the 1,N^2-propanodG lesion (Plum et al., 1992).

Impact of the 8-oxodG Lesion and the Opposing Base on Thermal Stability

UV melting profiles were used to evaluate the influence of the 8-oxodG lesion and the opposing base on duplex thermal stability. Table 1 lists the relevant T_m data. All melting measurements were made at the same DNA concentration, so T_m differences (ΔT_m) do not trivially reflect concentration dependent effects. Note that lesion incorporation can thermally destabilize or stabilize the duplex relative to its lesion-free counterpart, with the impact depending on the base opposite the lesion. These trends in the data are elaborated on in the subsections which follow.

The G Lesion Reduces Duplex Thermal Stability Relative to the Corresponding Lesion-Free Duplex When C, G, or T Are the Cross-Strand Partners, with No Apparent Correlation between Thermal and Structural Data.* Inspection of the data in Table 1 reveals that when the central dG residue opposite dC is replaced by dG*, the T_m decreases by 3.2 °C ($\Delta T_m = -3.2 \pm 0.4$ °C). In other words, the G*C duplex is 3.2 °C less thermally stable than the GC duplex, a result which is consistent with the findings of several other groups (Oda et al., 1991; Koizume et al., 1994; McAuley-Hecht et al., 1994). Despite this lesion-induced decrease in thermal stability, X-ray crystallography (Lipscomb et al., 1995) and NMR evidence (Oda et al., 1991; D. J. Patel, personal communication) suggest that the Watson–Crick geometry is maintained at and adjacent to the lesion site in an overall B-form duplex. *Thus, apparent structural identity cannot be used to infer that the two duplexes will exhibit equivalent thermal stabilities.*

The data in Table 1 also show that the T_m's of the G·G and G·T unmodified duplexes are reduced by incorporation of the dG* lesion, albeit to a lesser extent, with ΔT_m values of -1.7 ± 0.4 and -1.0 ± 0.4 °C, respectively. This rather marginal lesion-induced decrease in T_m is somewhat surprising considering that the CD spectra of the lesion-containing duplexes, while remaining B-like, nevertheless exhibit real differences relative to their corresponding lesion-free duplexes. These CD differences may reflect some redistribution of electrons in the bases (alternate tautomers) or conformational rearrangements in the vicinity of the lesion. *Thus, apparent CD detected differences cannot be used to infer significant differences in thermal stability.*

The G Lesion Increases Duplex Thermal Stability Relative to the Corresponding Lesion-Free Duplex When A Is the Opposing Base.* In contrast to the other three lesion-opposing residues, when dA is placed opposite dG* rather than dG (the G*A duplex vs the GA duplex), we observe an *increase* in thermal stability. Specifically, the T_m for the G*·A duplex is 7.6 ± 0.4 °C higher than that for the GA duplex. This enhanced thermal stability may reflect macroscopically the microscopic observation that the presence of the lesion induces a glycosidic rotation which produces an 8-oxodG(syn)·dA(anti) conformation at the lesion site (Kouchakdjian et al., 1991). However, as previously shown (Plum et al., 1992), such structural accommodations do not always lead to an increase in thermal stability.

In the Absence of the G Lesion, the Opposing Base Has a Much Greater Impact on Duplex Thermal Stability.* Inspection of the T_m data in Table 1 for the subset of DNA duplexes which do not contain the lesion reveals that the thermal stability of the duplex is reduced significantly relative to the parent GC duplex when the cross-strand partner base is A, G, or T. Note that the GG and GT duplexes display an approximately 8–9 °C reduction in T_m, while the GA duplex is destabilized thermally by 12.0 ± 0.4 °C. Such reductions in thermal stability are consistent with previous reports on duplexes in which the Watson–Crick base pairing scheme is disrupted by mismatched bases (Gaffney & Jones, 1989; Aboul-ela et al., 1985). Significantly, the magnitudes of these effects are much greater than those we observe for the lesion-containing duplexes. In other words, *the presence of the lesion reduces the influence of the opposing base on duplex thermal stability.*

Lesion Effects on the Duplex Transition Enthalpy

We just described the impact of the lesion and the opposing base on duplex thermal stability. However, the thermal melting temperature is not a thermodynamic parameter. Contrary to common practice, in the absence of enthalpy data, T_m measurements cannot be interpreted in terms of free energy changes. To understand the thermodynamic impact of a lesion, enthalpy data must be obtained. To this end, we have extracted the model-dependent van't Hoff enthalpy data from both optical and calorimetric transition curves and model-independent calorimetric values from heat capacity measurements.

The Three Model-Dependent van't Hoff Enthalpies Exhibit Differences. Model-dependent van't Hoff transition enthal-

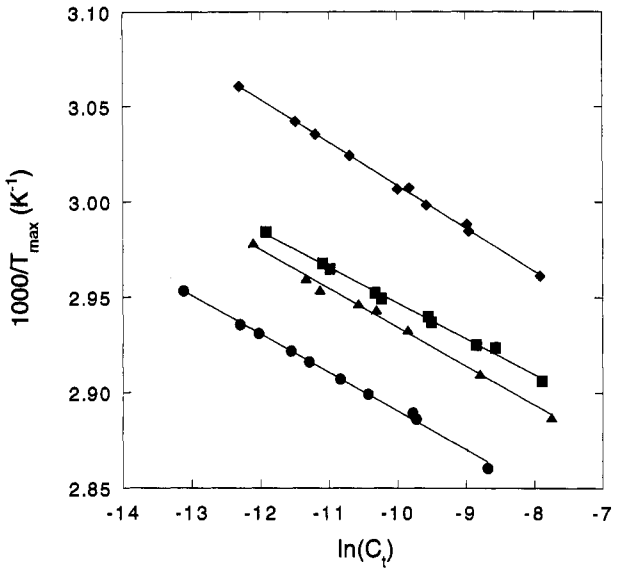

FIGURE 2: Concentration dependence of the optically monitored duplex melting transition. Symbols are defined as follows: GC (●), G*C (▲), GA (◆), G*A (■).

pies computed from the optical data are listed in the final two columns of Table 1. The ΔH_{vH}^{shape} data in column 3 result from analysis of the shape of the UV melting curves (eq 1). The values listed are averages from melts over a nearly 100-fold concentration range (~4 × 10^{-6} to ~4 × 10^{-4} M) and, within error, are independent of concentration. The van't Hoff enthalpies derived from the concentration dependence of T_{max} are listed in the final column of the table (ΔH_{vH}^{slope}). These data were determined from the slopes of the plots shown in Figure 2 by application of eq 3. We note that the van't Hoff enthalpies obtained by this slope method are systematically larger than those obtained by analysis of the shape of the optical curves. Recently, Koizume et al. (1994) published van't Hoff enthalpies for the melting of a series of molecules with dG or dG* placed opposite dA, dC, dG, and T. Their data were derived from $1/T_m$ vs $\ln(C_t/4)$ curves, where only a 6-fold range of DNA concentration was used, in contrast to the 100-fold range employed in this work. Direct comparisons between the data of Koizume et al. (1994) and those presented in this report are problematic due to differences in sequence context, the small concentration range covered in their study, and our observation of the failure of the van't Hoff model for the oligonucleotides studied here (see below).

We derived yet another set of van't Hoff enthalpies, ΔH_{vH}^{cal}, by analyses of the shapes of the DSC thermograms. These data are included in Table 2. Although these values are similar to those computed from the shapes of UV melting curves, the calorimetric van't Hoff enthalpies, with a couple of exceptions, tend to be somewhat larger. Such differences in van't Hoff enthalpies observed by optical and calorimetric techniques previously have been noted (Breslauer, 1986) and may reflect differing sensitivities of these observables to the progress of the duplex dissociation process.

An overall comparison of the three sets of van't Hoff transition enthalpies reveals significant differences. Particularly noteworthy is the fact that the values derived from the concentration dependent data are systematically higher than either set of values derived from the two shape analyses.

Table 2: DSC Derived Calorimetric and van't Hoff Transition Enthalpies for a Family of DNA Duplexes with and without the 8-oxodG Lesion

duplex	[single strand] (M × 10^4)	T_{max} (°C)	ΔH_{cal} (kcal/mol)	ΔH_{vH}^{cal} (kcal/mol)
G•C	3.76	75.8 ± 0.2	96.9 ±1.9	88.2 ± 2.5
G*•C	4.34	73.7 ± 0.2	89.6 ± 1.8	91.0 ± 2.7
G•A	3.62	64.5 ± 0.2	71.6 ± 2.9	76.5 ± 2.0
G*•A	3.98	70.7 ± 0.2	88.1 ± 1.8	95.1 ± 3.0
G•G	3.90	67.1 ± 0.2	100.9 ± 2.0	75.2 ± 1.9
G*•G	3.88	64.8 ± 0.2	102.7 ± 2.1	83.2 ± 2.4
G•T	4.24	67.3 ± 0.2	89.6 ± 1.9	76.3 ± 2.0
G*•T	4.82	65.8 ± 0.2	99.6 ±1.9	86.3 ± 2.6

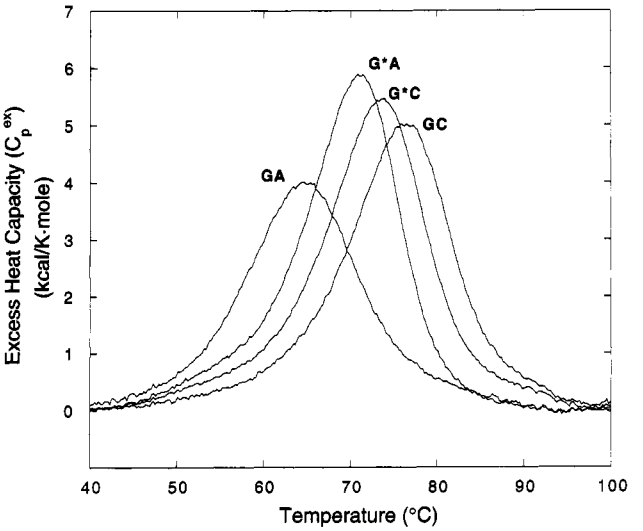

FIGURE 3: Representative differential scanning calorimetric melting profiles of DNA duplexes with and without the 8-oxodG lesion. Thermograms are labeled according to the convention described in the text.

These apparent inconsistencies between van't Hoff enthalpies determined by different methods indicate failure of one or more of the assumptions underlying the van't Hoff model. These failures may alter the apparent enthalpies differently depending on the method of calculation. For these reasons, it is desirable to use calorimetric techniques to determine directly and in a model-independent fashion the enthalpy data of interest.

Model-Independent Calorimetric Enthalpies. Figure 3 shows representative DSC thermograms (C_p^{ex} vs T curves). The T_{max} values derived from these C_p^{ex} curves are in excellent agreement with the corresponding temperatures obtained from UV melting studies at identical concentrations. We found the shapes of the thermograms to depend on the presence or absence of the lesion, as well as the identity of the opposing base; these dependencies are reflected in the van't Hoff enthalpies, which were discussed above. The area under each calorimetric melting profile corresponds to the model-independent transition enthalpy. These ΔH_{cal} values are listed in column 4 of Table 2. In our data analysis protocols (see Materials and Methods), the heat capacity at high temperature returns to the same value as at low temperature ($\Delta C_p = 0$), a feature consistent with previous calorimetric studies on nucleic acid transitions (Breslauer et al., 1986). Thus, for the duplexes studied here, we can compare directly transition enthalpies measured at different T_{max} values.

In the Absence of the Lesion, Creation of Mismatches at the Central GC Base Pair Can Dramatically Reduce or Increase the Dissociation Enthalpy, with the Direction and Magnitude of the Effect Being Dependent on the Cross-Strand Partner. Examination of the relevant data in Table 2 reveals that, for the GC, GA, GG, and GT duplexes, the calorimetrically derived transition enthalpies depend on the base opposite the central dG residue. Replacement of dC in the parent GC duplex by dA (GC vs GA) results in an extraordinary reduction of 25.3 ± 4.8 kcal/mol in the duplex transition enthalpy ($\Delta\Delta H$). Replacement of the opposing dC residue by dG or dT also leads to significant changes in the transition enthalpy ($\Delta\Delta H$) relative to the parent GC duplex. Specifically, the GG duplex enthalpically is 4.0 ± 3.9 kcal/mol more favorable than the GC duplex, while the GT duplex enthalpically is 7.3 ± 3.8 kcal/mol less favorable than the GC duplex. In short, relative to the parent GC duplex, the transition enthalpy of the lesion-free duplexes can be perturbed by as much as 25 kcal/mol just by creating a mismatch at the central G residue. The magnitude of this effect is remarkable because it represents a loss of ~26% of the total enthalpy of dissociation of the parent duplex, when only 1 of 13 base pairs is altered. On the basis of nearest neighbor predictions (Breslauer et al., 1986), complete removal of the central base pair is expected to reduce ΔH by ~21%. Thus, creation of a single mismatch can be more deleterious energetically than the complete loss of stacking on both sides of the normal base pair at that site.

*In the Presence of the Lesion, Creation of "Mismatches" at the Central G*C Base Pair Can Result in an Increase (dG, dT) or Can Have No Effect (dA) on the Dissociation Enthalpy.* For the subset of four duplexes with the lesion (G*C, G*A, G*G, and G*T), a different pattern emerges. Specifically, replacement of dC in the G*C duplex by dA (G*C vs G*A) does not alter significantly the duplex to single strand transition enthalpy ($\Delta\Delta H = -1.5 \pm 3.6$). This observation is in stark contrast to the same dC to dA replacement opposite the unmodified dG residue, which induces an extraordinary 25.3 ± 4.8 kcal/mol reduction in ΔH. These effects, however, are strongly dependent on the opposing base. By contrast to the near zero $\Delta\Delta H$ value for G*A relative to G*C, both G*G and G*T exhibit significantly larger transition enthalpies relative to G*C ($\Delta\Delta H = +13.1 \pm 3.9$ and $+10.0 \pm 3.7$ kcal/mol, respectively). Clearly, *the presence of the lesion significantly alters the impact of the cross-strand partner on duplex melting energetics.*

In the above examination of the effect of mismatches on the melting enthalpies of lesion-free and lesion-containing duplexes, we used either the GC or the G*C duplex as the thermodynamic reference. These comparisons represent the approach that is traditionally used in such studies. However, it also is instructive to compare each lesion-containing duplex to its corresponding lesion-free duplex (e.g., GA to G*A, GT to G*T, etc.) so as to isolate and define the thermodynamic impact of lesion incorporation. Consequently, in the following section, we refer to hypothetical transformations between nonlesion-containing and lesion-containing duplexes (e.g., GA ⇒ G*A).

Depending on the Cross-Strand Partner, Lesion Incorporation Can Reduce (dC), Increase (dG), or Not Perturb (dA, T) the Duplex Dissociation Enthalpy Relative to the Corresponding Lesion-Free Duplex. The data listed in Table 2 reveal that the impact of the lesion on duplex dissociation energetics is dependent on the cross-strand partner. To be specific, when opposite dC, replacement of the central dG residue by the dG* lesion (GC ⇒ G*C) enthalpically destabilizes the duplex by 7.3 ± 3.7 kcal/mol. Contrarily, relative to the corresponding unmodified duplex, the enthalpic impact of placing the dG* lesion opposite the other three cross-strand partners can be either neutral, as in the case of the G·G to G*·G transition ($\Delta\Delta H = 1.8 \pm 4.1$ kcal/mol), or significantly favorable, as in the G·A to G*·A and G·T to G*·T transitions ($\Delta\Delta H = 16.5 \pm 4.7$ kcal/mol and $\Delta\Delta H = 10.0 \pm 3.8$ kcal/mol, respectively). The near zero change in enthalpy associated with the G·G to G*·G transition is surprising in light of the nontrivial changes in structure implied by the circular dichroism spectra. This latter observation further emphasizes the lack of a simple predictive correlation between structure and thermodynamics.

Nature of the Transitions

Comparisons between the model-independent calorimetric enthalpy data and the model-dependent van't Hoff enthalpies traditionally are used to gain insight into the nature of a duplex melting process. Recall that the mole unit for the ΔH_{cal} data refers to the actual amount of duplex present in solution. By contrast, the mole unit for the ΔH_{vH} data refers to the fraction of the duplex that melts cooperatively (the so-called cooperative unit), which may or may not correspond to the entire duplex. If a melting process is indeed two-state, the size of the cooperative unit coincides with the actual size of the duplex and, therefore, $\Delta H_{vH} = \Delta H_{cal}$. This equivalence of van't Hoff and calorimetric enthalpies typically is observed for short oligonucleotides (≤8 bp) closed at each end by GC base pairs; however, these two enthalpy values may differ significantly for longer duplexes (Breslauer et al., 1986).

For the family of duplexes currently under investigation, we find that the van't Hoff enthalpies derived from the concentration dependence of T_{max} differ from the van't Hoff enthalpies derived from the shapes of the UV melting curves. Specifically, the van't Hoff values may be less than (G*C, GA, G*A), approximately equal to (GC, GT, G*T), or greater than (GG, G*G) the model-independent calorimetric enthalpy values. We describe below how one can combine optical and calorimetric data to take advantage of the strengths of both methods and to avoid the systematic error in the van't Hoff approach we observe for some lesion or mismatch-containing duplexes.

For the van't Hoff model, the concentration dependence of T_{max} depends on ΔH and n, since $\partial(1/T_{max})/\partial \ln C_t = R(n - 1)/\Delta H$. Because we have determined ΔH calorimetrically, we can fix ΔH to this value and compute an effective molecularity, n_{eff}, for each duplex. As we previously have discussed (Pilch et al., 1995), the resulting value of n_{eff} absorbs any deviations from the assumed van't Hoff model. Previously, we used a similar approach to assess the molecularities of higher-order DNA structures (Jin et al., 1990). For the duplexes studied here, our calculations of n_{eff} reveal significant deviations from bimolecular behavior. These deviations are not sufficiently large to question whether the complexes are two stranded (a fact already confirmed by mixing curves) but rather indicate the failure of the van't Hoff model to adequately describe these

Table 3: Free Energy Change for the Melting of a Family of DNA Duplexes with and without the 8-oxodG Lesion Derived from a Combination of Calorimetric and Concentration Dependent Optical Melting Data

duplex	T_{max}[a] (°C)	n_{eff}	ΔG (kcal/mol) 25 °C
G·C	76.0 ± 0.2	1.98 ± 0.04	19.3 ± 0.3
G*·C	73.5 ± 0.2	1.92 ± 0.06	17.3 ± 0.4
G·A	64.8 ± 0.2	1.81 ± 0.02	12.5 ± 0.4
G*·A	70.7 ± 0.2	1.83 ± 0.04	15.9 ± 0.3
G·G	67.1 ± 0.2	2.27 ± 0.11	19.3 ± 0.5
G*·G	64.8 ± 0.2	2.20 ± 0.08	18.4 ± 0.4
G·T	67.1 ± 0.2	2.03 ± 0.07	16.7 ± 0.4
G*·T	65.3 ± 0.2	2.04 ± 0.10	17.2 ± 0.5

[a] T_{max} adjusted for a DNA concentration of 4.0×10^{-4} M single strands.

molecules. Values for the effective molecularity, n_{eff}, are tabulated in Table 3.

The observed deviations from behavior consistent with the van't Hoff model may provide some insight into the melting process. The ΔH_{vH}^{shape} values described above are relatively insensitive to the molecularity of the transitions. In contrast, ΔH_{vH}^{slope} is very sensitive to molecularity. Because the melting/annealing process is governed by a balance between initiation (a bimolecular process) and propagation (a monomolecular process), apparent deviations in molecularity probably indicate anomalies of initiation. Interestingly, the values we find for the effective molecularity depend more strongly on the nucleotide opposite dG or dG* than on the presence or absence of oxidative damage. Thus, the unusual features of the melting process which are manifest in the differences between the formal and effective molecularities that we observe do not appear to be dictated by the presence or absence of the lesion.

Taken together, the observation of $\Delta H_{vH}^{shape} < \Delta H_{cal}$ and the anomolously weak concentration dependence of T_{max} (large ΔH_{vH}^{slope}) indicate significant deviations from the assumptions inherent in the van't Hoff model. Previously, we have noted such disparities and have proposed that they might reflect a more general predisposition toward melting of some lesion-containing and some apparently normal duplex domains (Pilch et al., 1995). At the very least, these significant deviations from melting behavior consistent with the van't Hoff model emphasize the advantages of direct, model-independent calorimetric determinations of duplex transition enthalpies.

Impact of the Lesion on Duplex Transition Free Energies

The T_m and ΔH data listed in Table 3 can be combined to evaluate the impact of the lesion on the duplex free energy. In Table 4, we make comparisons between the free energy changes associated with disruption of the various lesion containing and non-lesion containing duplexes. The data in Tables 3 and 4 reveal several interesting features which are elaborated on in the sections which follow.

*Formation of the Nascent G*C Lesion Site Is Destabilizing.* The G*C site can be considered to be a nascent lesion when it forms from oxidation of the guanine residue at a canonical Watson–Crick GC site. Inspection of the data in Table 4 reveals that such a modification of the central dG by addition of a carbonyl group to the 8-position of the guanine base (GC ⇒ G*C) destabilizes the duplex by 2.0 ± 0.7 kcal/mol

Table 4: Thermodynamic Impact of Mismatches and 8-oxodG Lesions

	$\Delta\Delta H$ (kcal/mol)	$\Delta\Delta G$ (kcal/mol) 25 °C
	8-oxodG	
GC ⇒ G*C	−7.3 ± 3.7	−2.0 ± 0.7
GA ⇒ G*A	16.5 ± 4.7	3.4 ± 0.7
GG ⇒ G*G	1.8 ± 4.1	−0.9 ± 0.9
GT ⇒ G*T	10.0 ± 3.8	0.5 ± 0.9
	Mismatches Relative to GC	
GC ⇒ GA	−25.3 ± 4.8	−6.8 ± 0.7
GC ⇒ G*A	−8.8 ± 3.7	−3.4 ± 0.6
GC ⇒ GG	4.0 ± 3.9	0.0 ± 0.8
GC ⇒ G*G	5.8 ± 4.0	−0.9 ± 0.7
GC ⇒ GT	−7.3 ± 3.8	−2.6 ± 0.7
GC ⇒ G*T	2.7 ± 3.8	−2.1 ± 0.8
	Mismatches Relative to G*C	
G*C ⇒ G*A	−1.5 ± 3.6	−1.4 ± 0.7
G*C ⇒ G*G	13.1 ± 3.9	1.1 ± 0.8
G*C ⇒ G*T	10.0 ± 3.7	−0.1 ± 0.9

at 25 °C, with this destabilization being enthalpic in origin. This $\Delta\Delta G$ value of −2.0 ± 0.7 kcal/mol at 25 °C corresponds to an equilibrium preference for the GC duplex over the G*C duplex of about 30 to 1. The magnitude of this lesion-induced effect should be contrasted with the relatively small lesion-induced reduction in T_m or T_{max} of only 3 °C. The observed lesion-induced destabilization also should be contrasted with the fact that the GC and G*C duplex structures, as determined by NMR and X-ray crystallography, are virtually indistinguishable. These observations, once again, serve as warnings against using T_m or structural data to draw conclusions about thermodynamic stability. Because the structure of these two duplexes is, within the ability of NMR (Oda et al., 1991; Patel, personal communication) and X-ray crystallography (Lipscomb et al., 1995) to characterize it, unchanged by the lesion, it is tempting to speculate that the addition of the carbonyl causes solvent reorganization in the vicinity of the lesion, thereby contributing to the observed thermodynamic disparity of the GC and G*C duplexes, despite their purported structural similarity. The data presented here, however, cannot differentiate between this solvent-based speculation and other possibilities that may not be detected by NMR and crystallography, such as changes in the base stacking and pairing strengths due to alterations in the guanine electron density distribution upon addition of the carbonyl group. Such solvent- and solute-based microscopic interpretations are inextricably coupled. Both effects probably contribute to the observed macroscopic thermodynamic differences.

The G Lesion Is Stabilizing When dA Is the Opposing Residue.* The G*A site may be incorporated into DNA either by insertion of dA opposite dG* during replication or by faulty insertion of dG* (from dG*TP) opposite dA. Thus, the G*A lesion may result from failure to repair damage during replication or may be produced as a nascent lesion. Inspection of the GA and G*A data in Table 4 reveals that lesion formation opposite a dA residue at 25 °C results in an enthalpically driven ($\Delta\Delta H$ = 16.5 ± 4.7 kcal/mol), thermodynamically more stable ($\Delta\Delta G$ = 3.4 ± 0.7 kcal/mol) duplex state relative to the unmodified GA duplex. By contrast, when the lesion is placed opposite either dG or T, there is virtually no change in transition free energy. This surprising stabilizing influence of lesion formation opposite

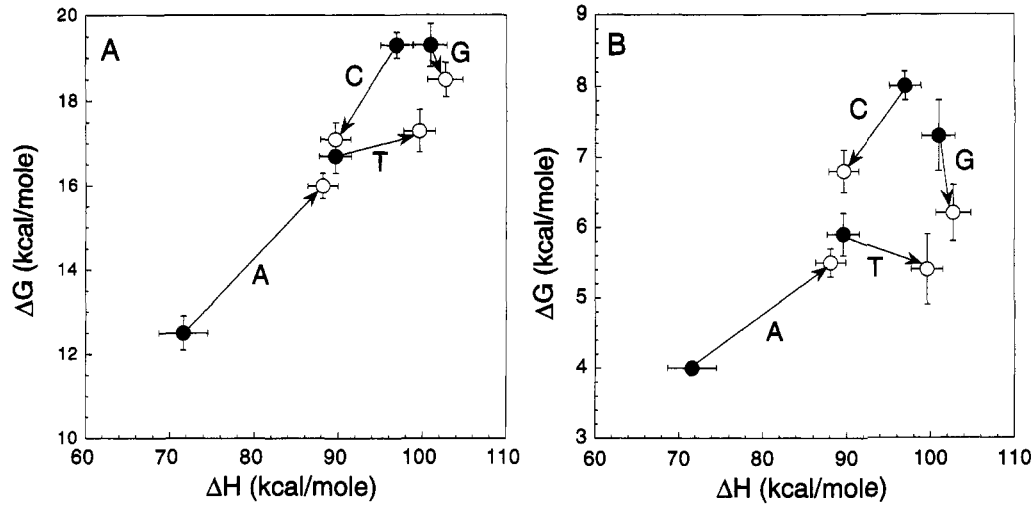

FIGURE 4: Thermodynamic impact of the 8-oxodG lesion represented in the $\Delta H-\Delta G$ plane at 25 °C (A) and 68 °C (B). Filled circles indicate dG whereas open circles indicate dG*; thus, the arrows originate at the undamaged duplexes and point to lesion containing duplexes. The arrows are labeled to indicate the cross-strand base.

dA probably reflects the *syn* structural accommodation of the lesion in the G*A duplex (Kouchakdjian et al., 1991; McAuley-Hecht et al., 1994). Note that, when opposite dA, the large enthalpic contribution of the lesion to duplex stability (16.5 ± 4.7 kcal/mol) is partially compensated by a large unfavorable entropy change, thereby resulting in a reduced but still rather significant lesion-induced stabilization of the duplex. Interestingly, this result contrasts with our observations of duplexes containing the 1,N^2-propanodG lesion (Plum et al., 1992), in which the *syn*−*anti* transition was found to be thermodynamically neutral. Again, it is possible that reorganization of solvent in the vicinity of the lesion may contribute to the large entropic effects.

Apparent Thermodynamic Similarity Does Not Imply Structural Similarity. Despite the substantial $\Delta\Delta G$ differences noted above for the G*C and G*A duplexes relative to their corresponding lesion-free duplexes, a direct comparison of the ΔG and ΔH values for disruption of these two duplexes at 25 °C reveals them to be strikingly similar (Table 4). This thermodynamic similarity is surprising because structural studies reveal a significant difference between the G*C and G*A duplexes, namely, a G*(anti)·C(anti) vs G*(syn)·A(anti) glycosidic conformation at the central lesion site. This result underscores a point that we previously have made (Plum et al., 1992; Plum & Breslauer, 1994), namely, *that large differences in structure do not necessarily correlate with large differences in thermodynamic parameters.*

The data on the GG ⇒ G*G and GT ⇒ G*T transitions provide additional examples of this point. Note that the relevant free energy differences between these pairs of duplexes ($\Delta\Delta G$) are, within experimental error, nearly zero. Thus, there appears to be no significant net free energy change associated with the apparent small but real structural alterations suggested by the quantitative differences in the corresponding CD spectra (Figure 1, panels C and D). It is interesting to note that this lack of differential free energy manifests itself differently in the two cases. The virtually isoergonic transition between dG and dG* in the GG mismatch duplex (GG ⇒ G*G) is the consequence of minimal compensating changes in ΔH and ΔS ($\Delta\Delta H$ = 1.8 ± 4.1 kcal/mol). By contrast, the GT system (GT ⇒ G*T) exhibits a large favorable change in enthalpy ($\Delta\Delta H$ = 10.0 ± 3.8 kcal/mol) and an almost exactly compensating change in entropy. Thus, apparent changes in structure may manifest themselves differently in terms of thermodynamics. In the aggregate, our results reveal that similar T_m's and even similar free energies may mask fundamentally different thermodynamic driving forces for a given pair of transitions.

Differences in Thermal Stability (ΔT_m) Do Not Necessarily Correlate with Differences in Thermodynamic Stability ($\Delta\Delta G$). Inspection of Table 4 reveals that, with the exception of the GA duplex, the transition free energy difference between the parent GC duplex and all of the other duplexes is virtually independent of the presence or absence of the lesion. By contrast, we noted earlier that the extent to which the T_m of any duplex is reduced relative to the parent Watson−Crick duplex depends on the presence or absence of the lesion, as well as the identity of the opposing residue, with ΔT_m values varying from 2 to 12 °C relative to the parent Watson−Crick GC duplex (see Tables 1 and 3 for T_m and T_{max} data). In the aggregate, these data dramatically demonstrate that melting temperature differences can be poor predictors of free energy differences. The GG mismatch provides a particularly striking example of this point. Due to differences in ΔH and the effective molecularity, the free energy impact at 25 °C of the GG mismatch is negligible, despite the fact that this mismatch significantly reduces the duplex melting temperature ($\Delta\Delta T_{max}$ = −8.9 ± 0.4 °C at 0.4 mM duplex concentration). This observation once again emphasizes the risk in assuming that changes in melting temperatures reflect changes in transition free energy at some temperature removed form the T_m (or T_{max}). In other words, thermal stability does not necessarily correlate with thermodynamic stability.

The Influence of the Lesion on Duplex Stability (ΔG) Depends on the Cross-Strand Partner and on the Temperature Chosen for Comparison. Figure 4A shows graphically the effect of addition of the 8-oxodG lesion on duplex thermodynamics at 25 °C in the $\Delta H-\Delta G$ plane. The arrows originate from the undamaged deoxyguanosine duplexes and point to the damaged 8-oxodeoxyguanosine duplexes. Note that, at 25 °C, lesion formation may be favorable (GA ⇒ G*A, GT ⇒ G*T) or unfavorable (GC ⇒ G*C, GG ⇒ G*G)

toward duplex stability. In short, the thermodynamic impact of the 8-oxodG lesion depends on the cross-strand partner.

Because calculation of ΔG depends on the value of ΔH (see eq 4), it is useful to make ΔG comparisons at more than one temperature (particularly one that minimizes extrapolation) to assess whether the free energy trends are trivial consequences of the selected temperature. In Figure 4B we examine the effects of the lesion in the $\Delta H-\Delta G$ plane at 68 °C, the mean T_{max}. For the most part, the effects observed at 25 °C of the central base pair on duplex thermodynamics are qualitatively maintained at 68 °C. However, due to the significant differences in ΔH values for the disruption of these duplexes, there are quantitative differences in the observed free energy changes. The most striking observation is that the value of $\Delta\Delta G$ for the GT ⇒ G*T transition changes sign. Thus, the introduction of the oxidative damage to a deoxyguanosine positioned across from T, which is thermodynamically favorable at low temperature, is unfavorable at elevated temperature.

Relative to the Corresponding Lesion-Free Duplexes, Lesion Incorporation Reduces the Dependence of Duplex Stability (ΔG) and Transition Enthalpy (ΔH) on the Cross-Strand Partner. The data plotted in Figure 4A and listed in Table 3 show that at 25 °C the range of free energy values observed for the duplexes without 8-oxodG is 6.8 ± 0.9 kcal/mol. Further inspection of these data reveal that this range is reduced dramatically to 2.5 ± 0.7 kcal/mol when the 8-oxodG lesion is present. A comparison of the thermodynamic impact of a mismatch of dG or dG* with dA is particularly striking. The GC ⇒ GA substitution is characterized by a large free energy difference ($\Delta\Delta G = -6.8 \pm 0.7$) which is the result of a dramatic and unfavorable difference in transition enthalpy ($\Delta\Delta H = -25.3 \pm 4.8$). In contrast, the G*C ⇒ G*A substitution is thermodynamically benign ($\Delta\Delta G = -1.4 \pm 0.7$, $\Delta\Delta H = -1.5 \pm 3.6$). Thus, the lesion serves to depress the dependence of duplex stability (ΔG) on the identity of the lesion-opposing base. In the absence of the lesion, the range of observed enthalpy values is 29.3 ± 4.9 kcal/mol. This ΔH range is reduced to 14.6 ± 3.9 kcal/mol when the lesion is present. We conclude therefore that the observed compression of ΔG values is both enthalpic and entropic in origin.

A trend toward entropic compensation of enthalpic differences among duplexes may be inferred from the observed small changes in free energy associated with relatively large changes in enthalpy. While we do not see evidence of linear enthalpy−entropy compensation behavior (Lumry & Rajender, 1970; Tomlinson, 1983), it is clear that the sometimes large enthalpy differences we observe for some duplexes relative to the parent GC duplex are partially suppressed in the free energy term by compensatory entropic effects.

Biological Consequences

In the sections that follow we discuss ways in which the results reported here can be used to gain insight into biological events in which lesion and mismatch containing duplexes participate.

Thermodynamic Anomalies May Contribute to Damage Recognition by Repair Enzymes. Most efforts to explain the basis of repair enzyme recognition of DNA lesion sites invoke a structural model. However, recall that the 8-oxodG lesion does not change the global Watson−Crick duplex geometry and imparts little if any structural change (other than the presence of the carbonyl group) to the G*C duplex relative to the unmodified parent GC duplex, thereby making structural discrimination alone unlikely as a basis for selective recognition. However, we find that the 8-oxodG•dC base pair does exhibit a significant thermodynamic impact on the G*C duplex in which it is housed, reducing its transition enthalpy by 7.3 ± 3.7 kcal/mol and its transition free energy by 2.0 ± 0.7 kcal/mol relative to the GC duplex. As we previously have discussed (Plum & Breslauer, 1994), this observation raises the possibility of energetic recognition. In fact, inspection of the data in Table 4 reveals that, with the exception of dG•dA, the free energy impact on duplex stability (ΔG at 25 °C) of an anomalous, noncanonical base pair relative to the parent dG•dC containing duplex falls within the range of ~0.0 to 3.4 kcal/mol of destabilization, independent of the presence or absence of guanine modification or the identity of the opposing residue. Perhaps these unfavorable free energy differences reflect a general feature of damaged and/or mismatched DNA which may be exploited by the repair machinery of the cell to identify regions of DNA which require repair, a possibility we previously have proposed (Plum & Breslauer, 1994; Pilch et al., 1995). Interestingly, the thermodynamic origins (ΔH and ΔS) of these similar lesion-induced or mismatch-induced free energy differences depend on the cross-strand partner base, a feature that may influence discrimination between various lesions by the cellular DNA repair machinery.

A Comparison of the Mut M Protein Binding Properties of Duplexes with and without the G Lesion and the Thermodynamic Properties of These Duplexes.* Castaing et al. (1993) and Tchou et al. (1994) have reported dissociation constants (K_d) for the complex formed by the Mut M protein (Fpg protein, 8-oxodG DNA glycosylase) and DNA duplexes containing the 8-oxodG lesion. Differences in solution conditions make problematic direct comparisons of our thermodynamic data to the binding data of Castaing et al. (1993) and Tchou et al. (1994). However, comparisons of the trends in duplex dissociation thermodynamics and the Mut M protein binding affinity may provide some insight into the recognition of the lesion by the repair enzyme. We define a preferential protein binding free energy as $\Delta\Delta G_b = -RT \ln(K_d^{G*C}/K_d^{G*X})$, where X is A, G, or T. We find a rough negative correlation between $\Delta\Delta G_b$ and the $\Delta\Delta G_d$ of duplex dissociation. These data are plotted in Figure 5. This observation of an apparent negative correlation between $\Delta\Delta G_b$ and $\Delta\Delta G_d$ suggests that the specific recognition of oxidative damage by Mut M protein does not depend, as one might expect, on the free energy contribution of the damaged domain to the overall duplex stability. It should be noted in this context that the Mut M protein binding data for duplexes without 8-oxodG do not fall on the curve defined by the data presented in Figure 5. Thus, we conclude that for this set of duplexes there is no simple correlation between duplex dissociation thermodynamics and Mut M protein binding affinity. This observation is counter to the expectation that the ease with which a DNA duplex domain is disrupted might correlate with the ability of a repair protein to recognize and bind to a damaged domain.

As reflected by the data listed in Table 3, the G*A duplex is destabilized only slightly relative to the G*C, G*G and G*T duplexes. Consequently, the inability of Mut M protein to recognize and excise the 8-oxodG lesion opposite dA,

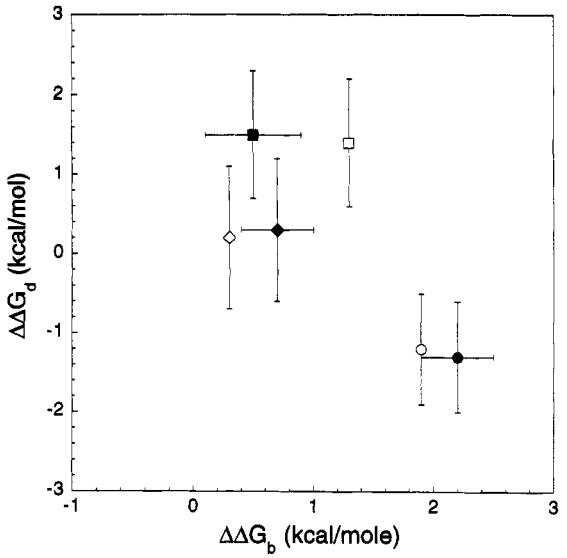

FIGURE 5: Comparison of the preferential Mut M protein binding free energy ($\Delta\Delta G_b$) to the free energy of DNA duplex dissociation relative to G*C ($\Delta\Delta G_d$). Closed symbols represent values calculated from the K_d data of Tchou et al. (1994) at 15 °C. Open symbols refer to values calculated from the K_d data of Castaing et al. (1993) at 20 °C for which no error estimates are provided by the authors. The cross-strand partner nucleotide is designated as follows: dA (●, ○), dG (■, □), T (◆, ◇).

when it efficiently removes the lesion opposite dC, T, or dG, cannot be rationalized *in toto* by differences in duplex free energies between these various duplexes. Discrimination may depend on structural features of the 8-oxodG·dA base pair (Grollman & Moriya, 1993; Grollman et al., 1994; Tchou et al., 1994), including the 8-oxodG(syn)·dA(anti) conformation observed by NMR and X-ray crystallography as well as perhaps the reorganization of solvent suggested by the large entropic impact of this lesion when it is opposite dA.

Finally, it may not be reasonable to expect correlations between the thermodynamics of disruption of DNA duplexes with interior lesions and the preferential insertion of deoxynucleotides opposite the lesions. Nevertheless, it is interesting to note that the dA and dC nucleotides, which are inserted preferentially by DNA polymerases opposite the 8-oxodG lesion (Shibutani et al., 1991; Grollman & Takeshita, 1995), produce duplexes which are enthalpically ($\Delta H \sim 89$ kcal/mol), but not ergonically ($\Delta G \sim 16.5$ kcal/mol), disfavored relative to duplexes with dT and dG opposite the lesion ($\Delta H \sim 100$ kcal/mol, $\Delta G \sim 18$ kcal/mol).

Concluding Remarks

In this work, we determined the thermodynamic and extrathermodynamic consequences of the 8-oxodeoxyguanosine lesion on duplex properties. We also compared these lesion-induced thermodynamic influences with the structural impact (Oda et al., 1991, Kouchakdjian et al., 1991; McAuley-Hecht et al., 1994; Lipscomb et al., 1995) and the biological impact (Floyd, 1990; Tchou & Grollman, 1993; Castaing et al., 1993) of the lesion. As we previously have shown (Vesnaver et al., 1989; Plum et al., 1992), such comparisons can provide insight into the biophysical impacts of DNA damage, while also allowing one to develop a better understanding of the complementary roles of structure and energetics in determining the biological consequences of DNA lesions, including their recognition and repair.

ACKNOWLEDGMENT

We thank Robert Rieger for the synthesis of the modified oligonucleotides.

SUPPORTING INFORMATION AVAILABLE

Derivation of equations for extraction of thermodynamic data from equilibrium melting curves of any molecularity in terms of T_{max} and tables of extinction coefficients (5 pages). Ordering information is given on any current masthead page.

REFERENCES

Aboul-ela, F., Koh, D., Tinoco, I., Jr., & Martin, F. H. (1985) *Nucleic Acids Res. 13*, 4811−4824.
Au, K. G., Clark, S., Miller, J. H., & Modrich, P. (1989) *Proc. Natl. Acad. Sci. U.S.A. 86*, 8877−8881.
Bessho, T., Tano, K., Nishimura, S., & Kasai, H. (1993a) *Carcinogenesis 14*, 1069−1071.
Bessho, T., Roy, R., Yamamoto, K., Kasai, H., Nishimura, S., Tano, K., & Mitra, S. (1993b) *Proc. Natl. Acad. Sci. U.S.A. 90*, 8901−8904.
Bessho, T., Tano K., Kasai, H., Ohtsuka, E., & Nishimura, S. (1993c) *J. Biol. Chem. 268*, 19416−19425.
Bevington, P. R. (1969) *Data Reduction and Error Analysis for the Physical Sciences*, McGraw-Hill, New York.
Bodepudi, V., Iden, C. R., & Johnson, F. (1991) *Nucleosides Nucleotides 10*, 755−761.
Bodepudi, V., Shibutani, S., & Johnson, F. (1992) *Chem. Res. Toxicol. 5*, 608−617.
Breslauer, K. J. (1986) in *Thermodynamic Data for Biochemistry and Biotechnology* (Hinz, H., Ed.) pp 402−427, Springer-Verlag, New York.
Breslauer, K. J., Frank, R., Blöcker, H., & Marky, L. A. (1986) *Proc. Natl. Acad. Sci. U.S.A. 83*, 3746−3750.
Bush, C. A. (1974) in *Basic Principles in Nucleic Acid Chemistry* (T'so, P. O. P., Ed.) Vol. 2, pp 91−169, Academic, New York.
Cadet, J., & Berger, M. (1985) *Int. J. Radiat. Biol. 47*, 127−143.
Cantor, C. R., & Schimmel, P. R. (1980) *Biophysical Chemistry*, Part 2, p 413, W. H. Freeman Co., San Francisco.
Castaing, B., Geiger, A., Seliger, H., Nehls, P., Laval, J., Zelwer, C., & Boiteux, S. (1993) *Nucleic Acids Res. 21*, 2899−2905.
Cheng, K. C., Cahill, D. S., Kasai, H., Nishimura, S., & Loeb, L. A. (1992) *J. Biol. Chem. 267*, 166−172.
Cho, B. P., Kadlubar, F. F., Culp, S. J., & Evans, F. E. (1990) *Chem. Res. Toxicol. 3*, 445−452.
Culp, S. J., Cho, B. P., Kadlubar, F. F., & Evans, F. E. (1989) *Chem. Res. Toxicol. 2*, 416−421.
Demple, B., & Harrison, L. (1994) *Annu. Rev. Biochem. 63*, 915−948.
Felsenfeld, G., & Rich, A. (1957) *Biochim. Biophys. Acta 26*, 457−468.
Floyd, R. (1990) *Carcinogenesis 11*, 1447−1450.
Fraga, C. G., Shienaga, M. K., Park, J.-W., Degan, P., & Ames, B. N. (1990) *Proc. Natl. Acad. Sci. U.S.A. 87*, 4533−4537.
Gaffney, B. L., & Jones, R. A. (1989) *Biochemistry 28*, 5881−5889.
Gajewski, E., Rao, G., Nackerdien, Z., & Dizdaroglu, M. (1990) *Biochemistry 29*, 7876−7882.
Gao, X., & Patel, D. J. (1988) *J. Am. Chem. Soc. 110*, 5178−5182.
Gralla, J., & Crothers, D. M. (1973) *J. Mol. Biol. 73*, 497−511.
Grollman, A. P., & Moriya, M. (1993) *Trends Genet. 9*, 246−249.
Grollman, A. P., & Shibutani, S. (1994) in *DNA Adducts: Identification and Biological Significance* (Hemminki, A., et al., Eds.) pp 385−397, IARC Science Publication No. 125.
Grollman, A. P., & Takeshita, M. (1995) in *Radiation Damage to DNA: Structure/Function Relationship of Early Times* (Fucidrelli, A. F., & Zimbrick, J. D., Eds.) pp 293−304, Batelle Press, Columbus OH.
Grollman, A. P., Johnson, F., Tchou, J., & Eisenberg, M. (1994) *Ann. N.Y. Acad. Sci. 726*, 208−214.
Halliwell, B., & Gutteridge, J. M. C. (1989) *Free Radicals in Biology and Medicine*, 2nd ed., Clarendon, Oxford.

Hayakawa, H., Taketomi, A., Sakumi, K., Kuwano, M., & Sekiguchi, M. (1995) *Biochemistry 34*, 89−95.
Hutchinson, F. (1985) *Prog. Nucleic Acid Res. Mol. Biol. 32*, 115−154.
Jin, R., Breslauer, K. J., Jones, R. A., & Gaffney, B. L. (1990) *Science 250*, 543−546.
Job, P. (1928) *Ann. Chim. (Paris) 9*, 113−134.
Kamiya, H., Murata-Kamiya, N., Koizume, S., Inoue, H., Nishimura, S., & Ohtsuka, E. (1995) *Carcinogenesis 16*, 883−889.
Kasai, H., & Nishimura, S. (1984) *Nucleic Acids Res. 12*, 2137−2145.
Kasai, H., & Nishimura, S. (1991) in *Oxidative Stress: Oxidants and Antioxidants* (Sies, H., Ed.) pp 99−116, Academic, London.
Koizume, S., Kamiya, H., Inoue, H., & Ohtsuka, E. (1994) *Nucleosides Nucleotides 13*, 1517−1534.
Kouchakdjian, M., Bodepudi, V., Shibutani, S., Eisenberg, M., Johnson, F., Grollman, A. P., & Patel, D. J. (1991) *Biochemistry 30*, 1403−1412.
Lindahl, T. (1990) *Mutat. Res. 238*, 305−311.
Lipscomb, L. A., Peek, M. E., Morningstar, M. L., Verghis, S. M., Miller, E. M., Rich, A., Essigmann, J. M., & Williams, L. D. (1995) *Proc. Natl. Acad. Sci. U.S.A. 92*, 719−723.
Lumry, R., & Rajender, S. (1970) *Biopolymers 9*, 1125−1227.
Maki, H., & Sekiguchi (1992) *Nature 355*, 273−275.
Marky, L. A., & Breslauer, K. J. (1987) *Biopolymers 26*, 1601−1620.
McAuley-Hecht, K. E., Leonard, G. A., Gibson, N. J., Thomson, J. B., Watson, W. P., Hunter, W. N., & Brown, T. (1994) *Biochemistry 33*, 10266−10270.
Michaels, M. L., & Miller, J. H. (1992) *J. Bacteriol. 174*, 6321−6325.
Michaels, M. L., Cruz, C., Grollman, A. P., & Miller, J. H. (1992a) *Proc. Natl. Acad. Sci. U.S.A. 89*, 7022−7025.
Michaels, M. L., Tchou, J., Grollman, A. P., & Miller, J. H. (1992b) *Biochemistry 31*, 10964−10968.
Mo, J.-Y., Maki, H., & Sekiguchi, M. (1992) *Proc. Natl. Acad. Sci. U.S.A. 89*, 11021−11025.
Moriya, M. (1993) *Proc. Natl. Acad. Sci. U.S.A. 90*, 1122−1126.
Moriya, M., & Grollman, A. P. (1993) *Mol. Gen. Genet. 239*, 72−76.
Moriya, M., Ou, C., Bodepudi, V., Johnson, F., Takeshita, M., & Grollman, A. P. (1991) *Mutat. Res. 254*, 281−288.
Oda, Y., Uesugi, S., Ikehara, M., Nishimura, S., Kawase, Y., Ishikawa, H., Inoue, H., & Ohtsuka, E. (1991) *Nucleic Acids Res. 19*, 1407−1412.
Pavlov, Y. I., Minnick, D. T., Izuta, S., & Kunkel, T. A. (1994) *Biochemistry 33*, 4695−4701.
Petersheim, M., & Turner, D. H. (1983) *Biochemistry 22*, 256−263.
Pilch, D. S., Plum, G. E., & Breslauer, K. J. (1995) *Curr. Opin. Struct. Biol. 5*, 334−342.
Plum G. E., & Breslauer, K. J. (1994) *Ann. N.Y. Acad. Sci. 726*, 45−56.
Plum, G. E., Grollman, A. P., Johnson, F., & Breslauer, K. J. (1992) *Biochemistry 31*, 12096−12102.
Privalov, P. L., & Potekhin, S. A. (1986) *Methods Enzymol. 131*, 4−51.
Puglisi, J. D., & Tinoco, I., Jr. (1989) *Methods Enzymol. 180*, 304−325.
Shibutani, S., Takeshita, M., & Grollman, A. P. (1991) *Nature 349*, 431−434.
Snell, F. D., & Snell, C. T. (1949) *Colorimetric Methods of Analysis*, 3rd ed., Vol. 2, p 671, Van Nostrand, New York.
Steenken, S. (1989) *Chem. Rev. 89*, 503−520.
Sturtevant, J. M. (1987) *Annu. Rev. Phys. Chem. 38*, 463−488.
Tchou, J., & Grollman, A. P. (1993) *Mutat. Res. 299*, 277−287.
Tchou, J., Kasai, H., Shibutani, S., Chung, M.-H., Laval, J., Grollman, A. P., & Nishimura, S. (1991) *Proc. Natl. Acad. Sci. U.S.A. 88*, 4690−4694.
Tomlinson, E. (1983) *Int. J. Pharm. 13*, 115−144.
Vesnaver, G., Chang, C.-N., Eisenberg, M., Grollman, A. P., & Breslauer, K. J. (1989) *Proc. Natl. Acad. Sci. U.S.A. 86*, 3614−3618.
Wood, M. L., Dizdaroglu, M., Gajewski, E., & Essigmann, J. M. (1990) *Biochemistry 29*, 7024−7032.
Wood, M. L., Esteve, A., Morningstar, M. L., Kuziemko, G. M., & Essigmann, J. M. (1992) *Nucleic Acids Res. 20*, 6023−6032.
Yeh, Y.-C., Chang, D.-Y., Masin, J., & Lu, A.-L. (1991) *J. Biol. Chem. 266*, 6480−6484.

BI951945+